

REPORT DOCUMENTATION PAGE

AFRL-SR-BL-TR-02-

Public reporting burden for this collection of information is estimated to average 1 hour per response, including the time for reviewing the data needed, and completing and reviewing this collection of information. Send comments regarding this burden estimate or reducing this burden to Washington Headquarters Services, Directorate for Information Operations and Reports, 1215 Jefferson Management and Budget, Paperwork Reduction Project (0704-0188), Washington, DC 20503

0043

aining
s for
ce of

1. AGENCY USE ONLY (Leave blank)		2. REPORT DATE January 7, 2002	3. REPORT TYPE AND DATES COVERED Final Technical Report: 03/31/99 to 03/31/01	
4. TITLE AND SUBTITLE DURIP: Equipment for Magnetically Controlled Air Plasma Processes			5. FUNDING NUMBERS AFOSR DURIP Grant #F49620-99-1-0210	
6. AUTHOR(S) Professor Richard B. Miles				
7. PERFORMING ORGANIZATION NAME(S) AND ADDRESS(ES) Princeton University Dept. Mechanical & Aerospace Engrg. Olden St. Princeton, NJ 08544			8. PERFORMING ORGANIZATION REPORT NUMBER	
9. SPONSORING / MONITORING AGENCY NAME(S) AND ADDRESS(ES) AFOSR/NA 801 North Randolph St. Room 732 Arlington, VA 22203-1977			10. SPONSORING / MONITORING AGENCY REPORT NUMBER	
11. SUPPLEMENTARY NOTES			AIR FORCE OFFICE OF SCIENTIFIC RESEARCH (AFOSR) NOTICE OF TRANSMITTAL DTIC. THIS TECHNICAL REPORT HAS BEEN REVIEWED AND IS APPROVED FOR PUBLIC RELEASE LAW AFR 190-12. DISTRIBUTION IS UNLIMITED.	
12a. DISTRIBUTION / AVAILABILITY STATEMENT Approved for public release; distribution is unlimited.			12b. DISTRIBUTION CODE	
13. ABSTRACT (Maximum 200 Words) The equipment purchased under this DURIP Equipment Grant was a 6.5 Tesla liquid helium-cooled superconducting magnet that was specially configured for studies of MHD flow control, power extraction, and thrust enhancement in supersonic air flows. The design of this magnet is unique in that the high magnetic field region lies at the center of a three-way cross. In the vertical direction, there is a two-inch diameter thru-hole to provide optical access or access to electrodes placed at the top and bottom of an MHD device. Each of the two horizontal directions are rectangular channels with approximately 3" x 3" clear access. This configuration provides the capability of installing external ionization devices that drive electrons along the magnetic field lines, which are orthogonal to the air flow path.				
14. SUBJECT TERMS Superconducting magnet, MHD flow Control, Power Extraction			15. NUMBER OF PAGES 10	
			16. PRICE CODE	
17. SECURITY CLASSIFICATION OF REPORT Unclassified	18. SECURITY CLASSIFICATION OF THIS PAGE Unclassified	19. SECURITY CLASSIFICATION OF ABSTRACT Unclassified	20. LIMITATION OF ABSTRACT UL	

20020221 057

FINAL TECHNICAL REPORT

AFOSR GRANT #F49620-99-1-0210

DURIP: Equipment for Magnetically Controlled Air Plasma Processes (150-6766)

Richard B. Miles
Department of Mechanical & Aerospace Engineering
Princeton University
Princeton, NJ 08544

January 7, 2002

ABSTRACT

The equipment purchased under this DURIP Equipment Grant was a 6.5 Tesla liquid helium-cooled superconducting magnet that was specially configured for studies of MHD flow control, power extraction, and thrust enhancement in supersonic air flows. The design of this magnet is unique in that the high magnetic field region lies at the center of a three-way cross. In the vertical direction there is a two-inch diameter thru-hole to provide optical access or access to electrodes placed at the top and bottom of an MHD device. In each of the two horizontal directions are rectangular channels with approximately 3" x 3.5" clear access parallel to the magnetic field and 3" x 3" perpendicular to the magnetic field. This configuration provides the capability of installing external ionization devices to drive electrons along the magnetic field lines, orthogonal to the direction of air flow. This unique configuration is accomplished by using a superconducting Helmholtz coil mounted at the base of a liquid helium/nitrogen dewar. A cross section schematic of the dewar and magnet configuration is shown in Fig. 1. A photograph of the magnet as installed in the laboratory is shown in Fig. 2. Fig. 3 shows the location of the magnet in the laboratory, and the 5 Gauss (0.0005 Tesla) measured field contour surrounding that magnet. The laboratory is approximately 25 feet wide by 31 feet long. The 5 Gauss line is approximately 19 feet from the magnet and represents the region within which safety procedures must be followed.

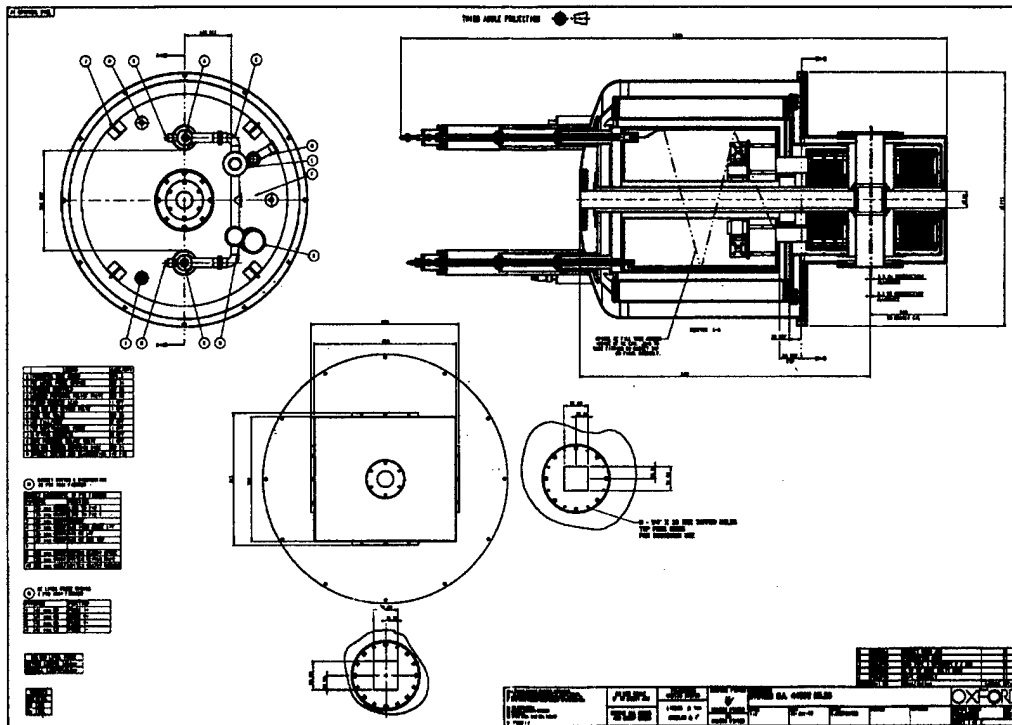


Figure 1. Cross section of the dewar and magnet configuration.

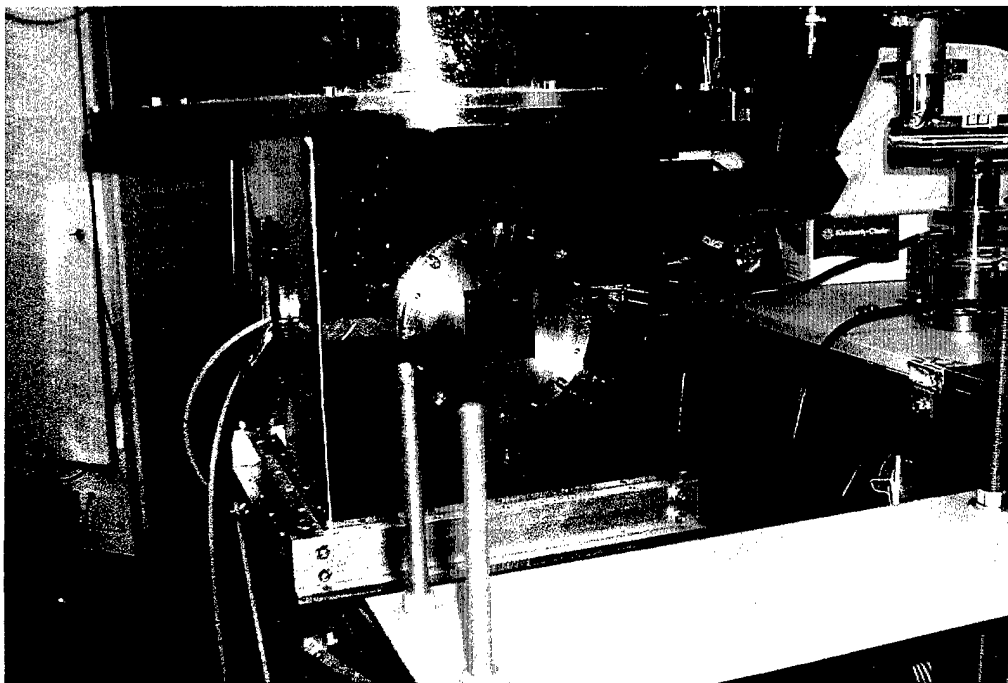


Figure 2. Photograph of the superconducting magnet within the laboratory (Room J-431 Engineering Quadrangle).

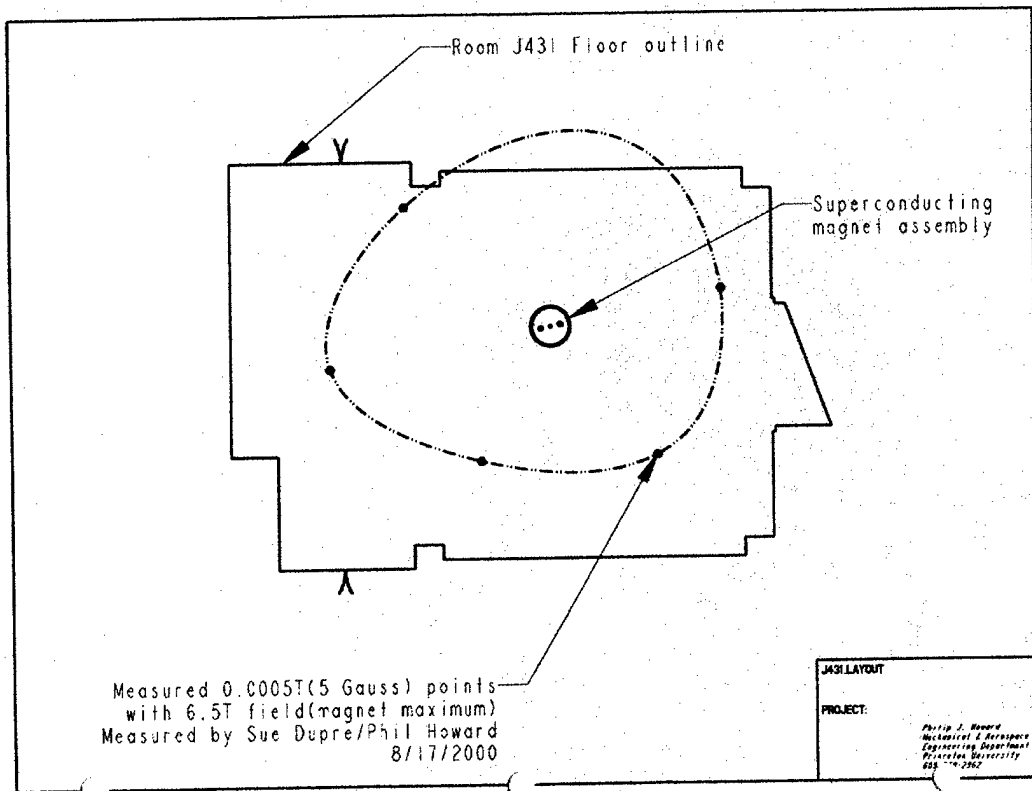


Figure 3. Location of the magnet within the laboratory (Room J-431 Engineering Quadrangle).

DISCUSSION

The magnet has been installed in the laboratory and tested. Preliminary studies have used the magnet to examine the effects of a magnetic field on the electrical breakdown threshold and arc formation in air. This is important because arc formation represents a serious limitation on the performance of MHD processes. Arcs can also cause serious degradation of electrodes through pitting and ablation. The presence of a strong magnetic field in a direction orthogonal to the arc causes it to move due to the Lorentz force. The geometry studied in this experiment was a cylindrical chamber with gas pressures ranging from 1 Torr to 500 Torr. The cathode of the cell was along the axis, with the anode forming a concentric ring around it. The end of the device was fitted with a window so arc formation could be observed from the laboratory. This coaxial electrode device was inserted into the magnet with the magnetic field lines along the z-axis. Arcs forming between the two electrodes are then orthogonal to the magnetic field.

The main observation from these experiments is that breakdown and arc formation are significantly suppressed. Fig. 4 shows a plot of breakdown voltage vs. chamber pressure for magnetic fields ranging from 0 to 6.5 Tesla. At pressures from 10 to 20 Torr (corresponding to atmospheric conditions in the range of high altitude flight) the 6.5 Tesla field is seen to increase the breakdown potential by a factor of approximately three. At lower pressures, there is also an extended range of glow discharge before arc formation occurs.

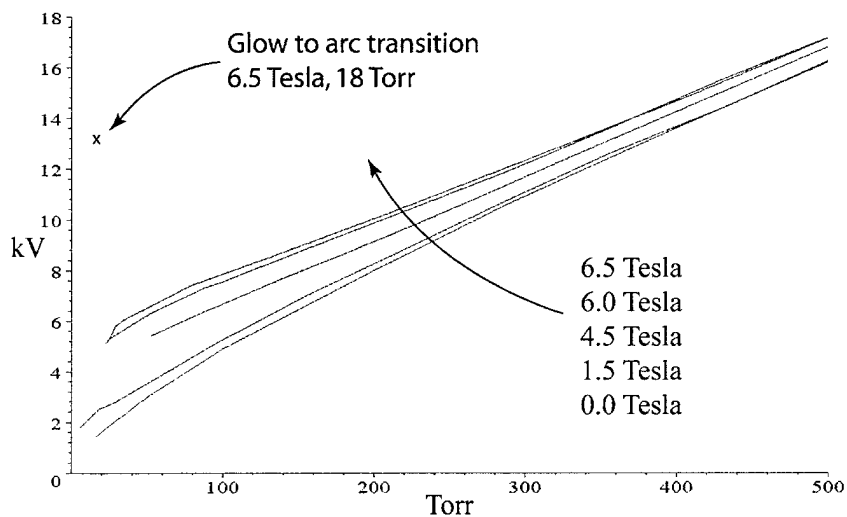


Figure 4. Breakdown threshold as a function of applied voltage and pressure for different magnetic field strengths.

The following images give insight as to how the physical form of the discharge is affected by the magnetic field. Fig. 5 shows images of the discharge at 18 Torr with varying magnetic field strengths. In each case, the electric field is increased as necessary to produce an arc. In Fig. 5a, with no field, the discharge is radial, steady, and somewhat contracted. As the field strength increases, the radial discharge begins to rotate at angular frequencies up to approximately 60 Hz for this setup. By 1.5 Tesla in Fig. 5b the voltage required to cause breakdown along with the reduced mobility of the electrons has caused the arc to become much more contracted, and unsteady. In this case (and at higher fields) the arc is curved but does not rotate. The multiple arcs seen in Figure 5b,c are likely due to the CCD exposure time and the unsteady nature of the discharge.

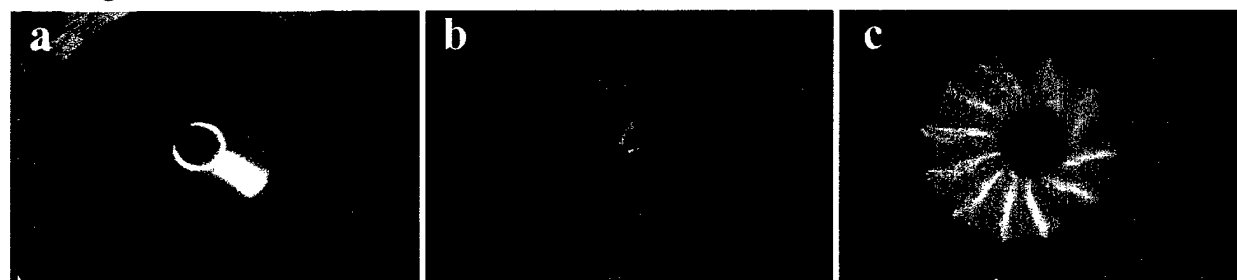


Figure 5. Discharge at 18 Torr, minimum arcing voltages and field strengths of 0.0 Tesla a.), 1.5 Tesla b.), and 6.5 Tesla c.).

Note: The apparent off center location of the cathode is due to aberrations in the lensing system required to remove the CCD camera as far as possible from the magnet.

Fig. 6 shows images of the discharge just before and after the glow to arc transition. The voltage applied in this case is on the order of 10 times the breakdown voltage without the magnet. It is interesting to contrast the diffuse, volume filling plasma suitable for MHD in Fig. 6a with the contracted discharge in Figure 5a at the same pressure with no magnetic field, and substantially reduced voltage.

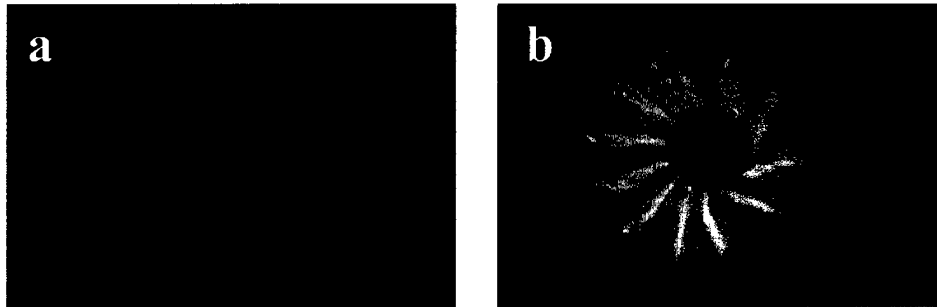


Figure 6. Discharge at 18 Torr, 6.5 Tesla, and 12.6 kV a), and 13 kV b).

It is clear, from this preliminary investigation, that in addition to providing the necessary Lorentz force for an MHD generator, the presence of the magnetic field significantly improves the “quality” of the breakdown by delaying arcing and maintaining a uniform, volume filling plasma.

MHD work in this magnet is awaiting the completion of an electron beam array that will be used to sustain the conductivity in low-pressure air. The construction of the electron beam array device is underway at Sandia Laboratories and Appendix 1 is a paper presented by the research staff members at Sandia Laboratories at the ICOPS 2001 Meeting on this electron beam array device. A Mach 4 low pressure wind tunnel that fits into this magnet is simultaneously under construction. MHD tests are expected to begin over the summer this year.

APPENDIX 1

1. Kim W. Reed, Gary E. Pena, Larry X. Schneider, and Joseph M. Rudys, "A Novel Electron gun with an Independently Addressable Cathode Array," ICOPS 2001, June 17-22, Las Vegas, NV.

A NOVEL ELECTRON GUN WITH AN INDEPENDENTLY ADDRESSABLE CATHODE ARRAY

Kim W. Reed, Gary E. Peña, Larry X. Schneider, Joseph M. Rudys
Sandia National Laboratories, Albuquerque NM 87185

Abstract

The design of a novel electron gun with an array of independently addressable cathode elements is presented. Issues relating to operation in a 6.5 Tesla axial magnetic field are discussed. Simulations with the TriComp [1] electromagnetic field code that were used to determine the space charge limited tube characteristic and to model focusing of the electron beam in the magnetic field are reviewed. Foil heating and stress calculations are discussed. The results of CYLTRAN [2] simulations yielding the energy spectrum of the electron beam and the current transmitted through the foil window are presented.

I. INTRODUCTION

This application requires that a vertical sheet electron beam be swept horizontally in a 6.5 Tesla axial magnetic field. Sweeping the beam in such a strong magnetic field is not an option, so the cathode was segmented in a horizontal array of vertical thermionic emitter stripes with a slotted grid that can be sequentially turned on from one side of the array to the other, Fig. 1.

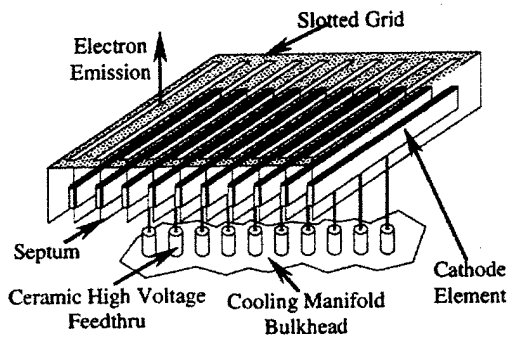


Figure 1. The cathode and grid structure.

The magnetic field is generated by a superconducting magnet with the electrical windings suspended freely in a liquid helium dewar. Since the windings are free to move in the dewar, any nearby magnetic shielding would pull

Sandia is a multiprogram laboratory operated by Sandia Corporation, a Lockheed Martin Company, for the United States Department of Energy under contract DE-AC04-94AL85000. This work is supported by Princeton University and the NSF.

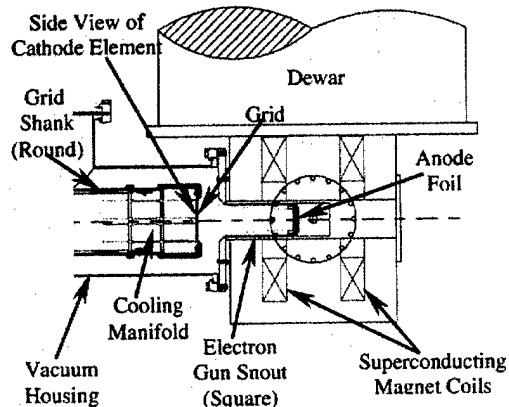


Figure 2. The electron gun and superconducting magnet.

the windings over to the wall of the dewar and quench the magnet. Therefore, in order to protect the electron gun control electronics from the Hall effect, they have to be located remotely, complicating the design. The magnet consists of a pair of toroidal windings on the same axis that produce a uniform axial magnetic field between them. A 7.62 cm x 7.62 cm square aperture opening runs through the magnet, centered on the axis of the windings. The electron gun must extend into this aperture so that the electron beam emerges from the foil window near the center of the magnet, Fig. 2. It is desired that the electron beam measure 5.08 cm x 5.08 cm at the foil window. The grid stalk is biased relative to the grounded foil window and outer vacuum housing with a DC voltage of -60 kV. If the grid stalk is too close to the outer housing, in order to maximize the area of the beam, the 6.5 Tesla magnetic field will prevent the high electric fields from initiating a breakdown, but corona emission will occur. The electrons will travel down the magnetic field lines resulting in a continuous dark current on the perimeter of the foil window. In addition to causing a cooling problem at the edge of the foil, this dark current would burden the high voltage power supply and the control electronics with a continuous current drain. This problem is addressed by locating the cathode in the larger vacuum region outside the magnet and then using the converging magnetic field to focus the beam onto the foil window.

The beam emerging from the foil in the center of the magnet must have an energy distribution that peaks at 30 keV and must have an adjustable current density in the sheet beams of 0 to 5 mA/cm². The sheet beams are

turned on by pulsing the cathode elements relative to the grid/septum structure, Fig. 1. The total duration of any given pulse is from 40 μ s to 5 ms.

II. THE TRIODE STRUCTURE

The electron gun consists of a triode structure with a thermionic cathode that is DC biased at $V_{cg} = 60$ kV. The rule of thumb for the maximum electrical stresses used in vacuum tubes is [3],

$$V/\text{gap} = k/(\text{gap}^{0.2}) \quad (1)$$

where,

$$V = \text{voltage on the gap [Volts]}$$

$$\text{gap} = \text{electrically stressed gap [meters]}$$

for a plane gap. For curved surfaces this electrical stress may be increased by a factor of 1.3. The value of the constant, k , is given in Table 1.

Table 1. k factor for electrical breakdown formula.

Pulse Length [μ s]	k
1	9.0×10^6
5	6.0×10^6
100	4.0×10^6
DC	3.0×10^6

According to this formulation, the maximum allowable field over the majority of the grid shank is about 99 kV/cm. The grid shank will be made of stainless steel, having a work function by contact potential of about 4.40. If it is desired to keep the dark current to less than 0.1 mA, so that it doesn't drag down the high voltage power supply, the allowable current density based upon the 5100 cm^2 grid stalk area would be 20 nA/ cm^2 . Using the Fowler-Nordheim theory [4] and 99 kV/cm, attaining this current corresponds to being able to condition the grid shank so that the height-to-width aspect ratio of the remaining whiskers be no more than 10 to 1. This is very reasonable. If the cathode were located at the end of the snout that extends into the magnet, this condition would only allow for the beam to be 3.81 cm x 3.81 cm. Conversely, with the cathode located in the large vacuum region, outside the magnet, a TriComp analysis using the electron tracking feature, shown in Fig. 3, indicates that the beam arriving at the foil, on the right side of the figure, can be 4.57 cm x 4.57 cm. The emission surface of the cathode was chosen to be 10.16 cm x 10.16 cm and the TriComp analysis was used to determine the required axial location of the emission surface so that the outermost electrons just skim the vacuum vessel. The electrons are following the magnetic field direction from the superconducting magnet, so it is not physically possible to make the beam emerging from the foil any larger. Locating the thermionic cathode remotely from the

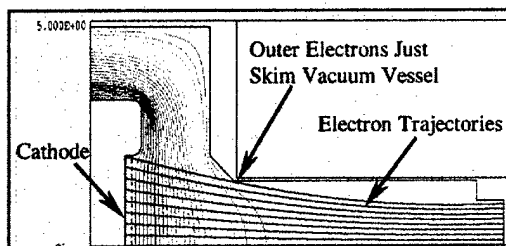


Figure 3. TriComp analysis showing the trajectories of the electrons emitted from the cathode.

foil window significantly reduces the static heat load on the foil, allowing the electron beam to be operated for longer bursts and with higher current densities.

The vacuum vessel outside the magnet is a standard 25.4 cm dia. tube, which allows the grid shank to be large while staying well below the allowable stress levels. The shank is 15.24 cm dia. The main reason, however, that this part of the vacuum vessel is so large is to maximize the pumping rate to the cathode region. Pumping rate is an issue because the BaCaO thermionic cathode must be operated at a vacuum of 10^{-7} Torr or better. The matter is further complicated by the fact that all high vacuum pumps that were investigated contained some magnetic materials. In addition, cleanliness issues with the cathode rule out diffusion pumps, eddy current forces rule out turbomolecular pumps and magnetic forces on ion trajectories rule out ion pumps. It was decided to use a cryovac and locate it remotely from the magnet – this necessitates the use of high conductance lines between the pump and cathode region.

Efficiency, grid heating and foil heating issues require that attention be given to achieving maximum transmission of the electron beam through all of the structures that are in its path. To take advantage of the strong axial magnetic field a slotted grid design was selected, as shown in Fig. 1. The grid is made of 0.076 cm thick molybdenum sheet with 0.208 cm wide x 10.16 cm long slots that lie directly over and are the same dimensions as the cathode emission elements. This arrangement provides 100% electron transmission through the grid and eliminates the additional heating of the grid that would occur if it intercepted part of the beam. Molybdenum was chosen because it has a high melting point, making it compatible with the radiant heating from the thermionic cathode. An Oxide dispenser cathode can supply about 20 mA/ cm^2 [5], exceeding the required 5 mA/ cm^2 when heated to about 600°K. This puts the grid/cathode region of the triode in the space charge limited regime.

Applying the TriComp code in the space charge limited emission mode allows the current density across the grid/cathode structure as a function of voltage to be modeled, Fig. 4. Notice the increase in the current density at the inner edges of the cathodes adjacent to the center

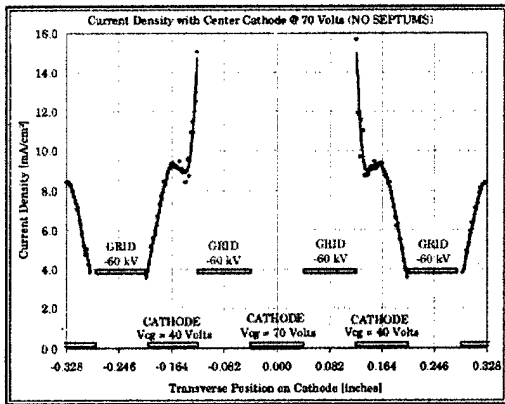


Figure 4. Intensification of the electrical field causes the current density to increase at the electrical potential bunching sites.

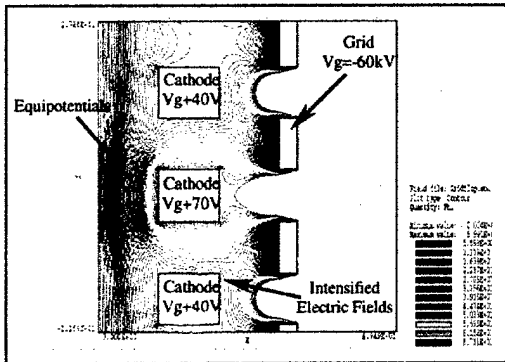


Figure 5. Electric fields from adjacent cathodes cause bunching of the equipotentials of nearest neighbors.

cathode that is turned off. This is caused by intensification of the electric fields at the corners of the cathodes that are adjacent to the center cathode due to its 30 Volt relative bias, Fig. 5. TriComp has served as a valuable tool, as this doubling in the current density at the edges of the two cathodes would have resulted in a broken foil window and a poisoned cathode. Further TriComp analysis shows that the cross talk between adjacent cathodes can be completely eliminated by placing a septum, at the same potential as the grid, between each of the cathodes. With the interaction between the cathode elements thus corrected, the transverse current distribution in the grid slots is roughly Gaussian.

III. THE TUBE CHARACTERISTIC

The approximate triode tube characteristic is [6],

$$I_a = P[V_{gc} + V_{ag}/\mu]^{3/2} \quad (2)$$

where,

- I_a = the current leaving the cathode.
- V_{gc} = the voltage of the grid relative to the cathode.
- V_{ag} = the anode voltage relative to the grid.
- P = the permeance of the tube.
- μ = a measure of how much the space charge limited flow in the cathode/grid region is influenced by the acceleration potential that reaches through the grid.

TriComp can be used to generate a plot of current density as a function of V_{gc} and V_{ac} . This is the tube characteristic, shown in Fig. 6.

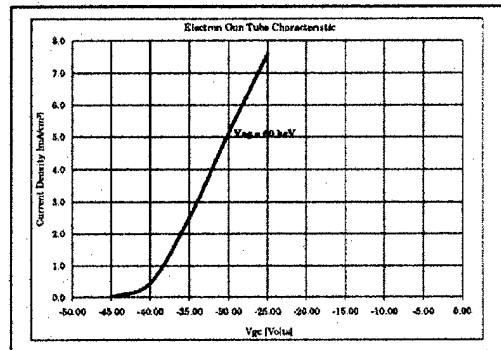


Figure 6. The triode tube characteristic determined from a series of TriComp runs with $V_{ag} = 60$ kV and various values of V_{gc} .

This electron gun is designed to operate at an acceleration potential of $V_{ag} = 60$ kV, so the tube characteristic was only calculated for that value of V_{ag} . Knowledge of the cathode voltage relative to the fixed potential of the grid that is required to turn the electron gun fully on to fully off is essential for selecting the bias power supplies and designing the control electronics. The data in Figure 6 revealed that the influence of the acceleration potential on the electrons in the region between the cathode and grid is so strong that the cathode will always be positive relative to the grid. Thus if the cathodes were biased positively relative to the high-voltage deck, then the grid could be at the potential of the high-voltage deck eliminating the need for a grid bias supply.

IV. THE ELECTRON BEAM WINDOW

It is desired to generate an electron beam out of the beryllium foil window with a current density in the beam that is adjustable from 0 to 5 mA/cm², an energy distribution with a peak at 30 keV and a maximum pulse duration of 5 ms. The foil has to be as flat as possible on the output side and withstand a pressure differential of 1 atm. Any one of these requirements by themselves is easy to accomplish, but a low energy beam requires a thin

foil. Foil heating due to the relatively long pulse duration and high current density reduces the yield strength of the foil. Furthermore, the foil cannot be preformed, which greatly increases the tensile stresses it will experience.

CYLTRAN was used to determine the required Be foil thickness in order to obtain the desired energy distribution out of the foil for a given input acceleration potential. It was determined that an energy distribution that peaked at the desired 30 keV, Fig. 7, could be obtained using a 60 keV acceleration potential and a 0.00254 cm thick Be foil. The analysis showed that 54% of the impinging electrons would pass through the foil. Calculations indicate that with a proper design, a hibachi with about 50% transparency to the electrons could be built. Magnetic focusing yields a current density gain of five from the cathode to the foil. Therefore only about 3.8 mA/cm² is required from the cathode to achieve the required peak current density of 5 mA/cm² at the foil.

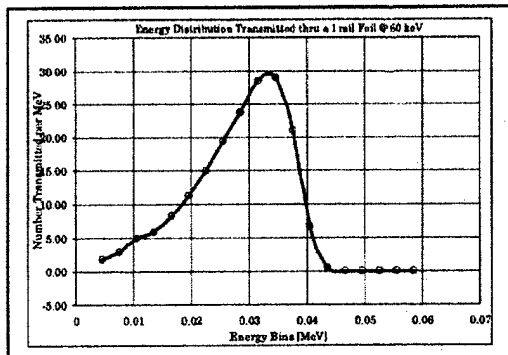


Figure 7. Results of a CYLTRAN run showing the energy distribution of the electron beam emerging from the 1 mil Beryllium foil.

Energy deposition in the foil was also determined from the CYLTRAN analysis. Specific heat, density, modulus of elasticity and yield stress were obtained as a function of temperature. Foil heating was then calculated from numerical integration and it was determined that the foil would reach 411°C and 45.5% of yield after a 5 ms pulse. A current density of 15 mA/cm² was initially proposed, but this analysis revealed that the foil wouldn't survive the longer pulse. Tensile stresses in the foil were calculated using formulations from Roark [7].

Heating of the stainless steel hibachi was calculated based upon energy depositions from CYLTRAN and the assumption that heating was adiabatic. This yielded a surface temperature of more than 4300°C at the end of the pulse, Fig. 8, which would result in ablation. This high temperature is due to the fact that all of the energy is deposited within 0.001 cm of the surface. In 5 ms, however, the energy diffuses out of this layer, so when thermal diffusion was included in the calculation it was found that the hibachi temperature would only rise to about 242°C.

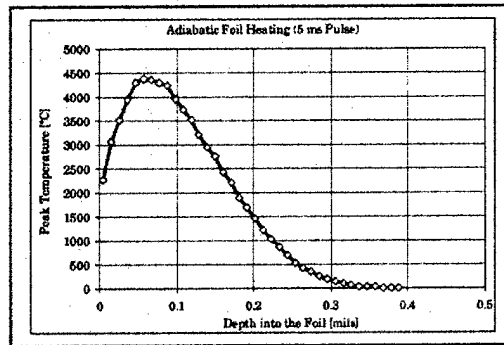


Figure 8. The energy distribution in the surface of the stainless steel hibachi, from CYLTRAN.

V. CONCLUSIONS

A brief overview of the design of a novel multi-cathode electron gun has been given. Some of the tools key to the design were discussed. Issues that complicated the design including the presence of a strong magnetic field, limited space at the output of the gun, cross talk between the independently pulsed cathodes and low energy of the beam were presented. The use of the design tools to solve these problems and the resultant solutions were discussed. Focus was on the most interesting problems and solutions and many issues and detailed calculations had to be omitted for brevity.

VI. REFERENCES

1. TriComp for Windows, Field Precision, PO Box 13595, Albuquerque, NM, (505) 296-6689, <http://www.fieldp.com>.
2. J. A. Halbleib, R. P. Kensek, T. A. Mehlhorn, G. D. Valdez, S. M. Seltzer and M. J Berger, "ITS Version 3.0: The integrated TIGER Series of Coupled Electron/Photon Monte Carlo Transport Codes," Sand Report: SAND91-1634, UC-405, March 1992.
3. The Handbook of Microwave Technology, Vol. 1 (1995). Particularly note the reference made to Armand Staprans at Varian cited on pg. 538.
4. Rod Latham, "High Voltage Vacuum Insulation," Academic Press, 1995, pp. 119-128, ISBN 0-12-437175-2.
5. J. W. Gewartowsky and H. A. Watson, "Principles of Electron Tubes," D. Van Nostrand Co., Inc., 1965, p. 42.
6. Willis W. Harman, "Fundamentals of Electronic Motion," McGraw-Hill Book Company, Inc., 1953, pp. 136-139, Library of Congress Catalog Card Number: 52-13456.
7. Warren C. Young, "Roark's Formulas for Stress & Strain," Sixth Edition, McGraw-Hill, Inc., 1989, pp. 477-478, ISBN 0-07-072541-1.